CFD MODEL VALIDATION OF A BAG FILTER FOR AIR FILTRATION IN A MILLING PLANT

Federico Solari[(a)], Giorgia Tagliavini[(b)], Roberto Montanari[(c)], Eleonora Bottani [(d)], Nicola Malagoli[(e)], Mattia Armenzoni[(f)]

[(b)]Interdepartmental Center CIPACK, University of Parma – Parco Area delle Scienze 181/A, 43124 Parma (Italy)

[(a),(c),(d),(e),(f)] Department of Engineering and Architecture, University of Parma – Parco Area delle Scienze 181/A, 43124 Parma (Italy)

[(a)]federico.solari@unipr.it, [(b)]giorgia.tagliavini@unipr.it, [(c)]roberto.montanari@unipr.it, [(d)]eleonora.bottani@unipr.it, [(e)]nicola.malagoli@unipr.it, [(f)]mattia.armenzoni@unipr.it

ABSTRACT

Milling plants often adopt pneumatic conveying to transport grains or flour inside their pipes.

The most common conveyor is air, which must be cleaned from solid particulate in suspension, before being released into the atmosphere.

To ensure air depuration, a filtration system is installed at the end of the milling plant. Such systems typically consist of cyclones separators and bag filters.

This paper presents the design and the validation of a computational fluid dynamic model for a pilot plant reproducing the mentioned air filtration system.

The pilot plant, located inside a laboratory at the University of Parma, was equipped with sensors to collect velocity and pressure data.

The comparison between the experimental values and those from the fluid dynamic simulations made the model validation possible and thereby achieving a robust predictive approach for the design of air filtration systems.

Keywords: Computational Fluid-Dynamics, Air Filtration, Bag Filters, Milling Industry

1. INTRODUCTION

In milling plants, granular products are often moved thanks to pneumatic transport. Consequently, the air used as a conveyor must be filtered before being released back into the atmosphere.

Filtration consists in the separation of different phases by inserting a filter media along the fluid path. Such a technique employed in many areas: from automotive to food industry [Billings et al. (1970), Sutherland (2008)].

The separation between solid and gas/liquid phase is influenced by the particles size or the particle density.

Cyclones separators have been the most common devices for removing dispersed particles from their carrying gases, thanks to their favorable balance of good separation efficiency and low cost of investment, operation and maintenance. Moreover, cyclones are able to handle any combination of gas pressure, temperature and several particles types. Therefore, they are considered more simple, robust and reliable than other separation equipment.

All the factors described above are crucial to make cyclone separators key components in different sorts of industrial plants for gas filtration [Alexander (1949), Chen et al. (2007)].

For this reason, since the 19th century, experimental studies have been developed to investigate the flow characteristics inside cyclones for a better understanding of pressure drops and separation efficiency [Meier et al. (1998), Stendal (2013)].

Filters are classified according to their ability to remove particles of a specific size. Fabric is the most widely used filter material. It is made from natural or synthetic fibers and typically requires some kind of support to be used as filter medium [Le Goff et al. (1969), Sommerfeld (2000)].

Bag filters are a type of filter frequently used for liquid or gas filtration. In the latter case, the units are significantly larger and multiple installations are needed, because of high flow rates [Lo et al. (2009), Mehta et al. (1956), Yoa et al. (2001)]. These filters are long cylindrical fabric hoses, mounted on a cylindrical cage with holding rings along the filter length. The hose is upright, closed at the bottom, hanging from a plate with the aperture at the top fastened to a hole in the plate.

Cyclones can usually reach high separation efficiencies, but despite this, they fail to separate the finest particles; to overcome this limit, it is necessary to combine them with bag filters, especially when it comes to air depuration.

In the research described in this paper, a bag fabric filter was installed inside a cyclone separator. This particular solution combines the cyclone and the filter benefits to enhance the separation efficiency with low energy consumption. Furthermore, this solution not only

improves the system overall efficiency, but also allows positive effects on filters operating conditions, increasing their life cycle. Ultimately, dust emission levels into the atmosphere are kept within the limits prescribed by law regulations.
The objective of this work was to study the behavior of this combined filtering system at different operating conditions with the purpose to obtain a predictive fluid dynamic model for industrial design. This was possible due to computational fluid dynamics simulations validated with a targeted experimental campaign on a pilot plant.

2. EXPERIMENTAL APPROACH AND THEORETICAL ASPECTS

The experimental campaign was conducted on the pilot plant built up inside the Industrial Engineering laboratory of the University of Parma, reproducing the mill filtration system previously described.
It consists of a bag fabric filter with 31 hoses placed inside a cyclone separator.
As this filtration system is not connected to a real industrial plant, it needs to exploit the air from the external environment. To do so, a suction fan controlled by an inverter draws the air inside the system. After passing through the filter, the air is recirculated in the atmosphere (Figure 1).

(a)

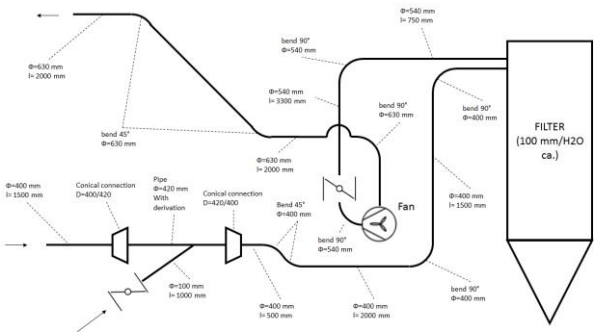

(b)

Figure 1: Pilot plant (a) and its scheme (b).

Since ambient air was used, which is free from solid particulate, the data collection and the subsequent simulations focused only on the fluid dynamic aspects of the system, omitting the separation efficiency at this first stages.

2.1. Data acquisition and sensors description

The velocities inside the filter were collected thanks to a hot-wire anemometer and a Pitot tube flow meter, while the pressure drop was measured with a differential pressure sensor.
To test the correct functioning of the pilot, the airflow rates were estimated. Due to the evaluation complexity, the airflow rates acquired experimentally were compared to those from the fan operating curve at different inverter frequency values.
For velocity and pressure data acquisition, appropriate housings were created to insert the sensors probes at various points along the filter as well as along the inlet and outlet ducts.
In particular, the housings were placed on the filter in the following points (Figure 2):

- one at the bottom of the cyclone, to collect the velocities (green dot);
- four at the volute of the cyclone to evaluate the velocities (yellow dots);
- one at the inlet and one at the outlet section for pressure drop (red dots).

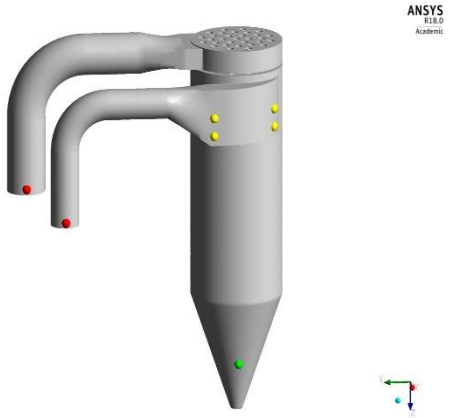

Figure 2: Sensor placement.

2.1.2. Hot-Wire Anemometer

A VelociCalc Air Velocity Meter 9565 Series was used. This instrument is commonly used to determine the air speed inside ventilation ducts.
It consists of a thermo-resistance, i.e. a resistor whose value is proportional to the temperature. This resistance is immersed in the tested flow. An electric current of known intensity keeps the resistance at a higher temperature compared to the fluid. The fluid cools the resistor proportionally to its velocity, allowing the data acquisition.
The advantages of this sensor are mainly associated to the reduced probe dimension. Hence, it allows to take measurements at various locations in the pipeline minimally affecting the fluid flow and ensuring a very quick response. Some drawbacks are related to calibration issues [VelociCalc Manual]. The main technical specifications are listed in Table 1.

Velocity (TA Probe)	
Range	0 to 50 m/s
Accuracy	±0.0015 m/s
Resolution	0.01 m/s
Temperature (TA Probe)	
Range	-10 to 60°C
Accuracy	±0.3°C
Resolution	0.1°C
Relative Humidity (TA Probe)	
Range	5 to 95% RH
Accuracy	±3% RH
Resolution	0.1% RH

Table 1: Hot-wire Anemometer technical specifications.

2.1.3. Pitot tube flow meter

The functioning of the Pitot tube grounds on the Bernoulli's equation (Equation 2).

$$p_{tot} = p_{st} + \frac{1}{2}\rho|\langle v\rangle|^2 \quad (2)$$

$$v = \sqrt{\frac{2(p_{tot}-p_{st})}{\rho}} \quad (3)$$

The Pitot tube is a simple sensor but reliable sensor: a tube with at least two holes is inserted within the fluid flow. The holes are the pressure probes, located respectively tangentially and orthogonally to the flow.
The first pressure probe measures the total pressure while the second one provides the static pressure. As the two separate channels converge towards a differential pressure gauge or a differential pressure transmitter, the dynamic pressure is calculated as the difference between the two detected pressures, which is proportional to the square of the fluid velocity (Equation 3).
The device used was a PCE PVM-620 Pitot tube, with the following technical specification (Table 2).

Pressure	±3735 Pa
Velocity	1.27 to 78.7 m/s
Resolution	1 Pa – 0.1 m/s
Accuracy	±1%

Table 2: PCE PVM-620 technical specifications.

2.1.4. Differential pressure sensor

The differential pressure sensor is an Endress Hauser Deltabar S PMD75, whose technical specifications are shown in Table 3.

Pressure	±10 mbar to ±40 bar
Temperature	-40 to +85°C
Output	4 to 20 mA
Accuracy	±0.035 %

Table 3: Deltabar S PMD75 technical specifications.

This sensor embodies process isolating diaphragms, which are deflected on both sides by the acting pressures. A filling oil transfers the pressure to a resistance bridge. The change in the bridge output voltage depends on the differential pressure, which can be measured and processed [Deltabar S PMD75 Manual] (Figure 4).

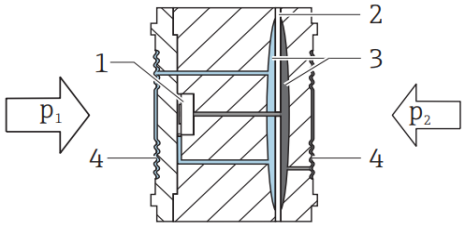

Figure 4: PMD75 measuring system: 1) measuring element, 2) middle diaphragm, 3) filling oil, 4) process isolating diaphragms.

2.2. Theoretical aspects of cyclone separators and filters

Cyclone separators draw the particles inside the fluid into a vortex, where inertia and gravitational forces act upon particles separation.
The fluid enters tangentially into the cylindrical chamber with a high rotational component. The flow descends rotating near the wall, until a certain location where the axial velocity component reverses itself, making the flow to ascend. The ascension proceeds near the cyclone axis [Cortés et al. (2007)].
As said above, it is helpful to understand how cyclones works but, in this case, their characteristic structure has not been strictly followed. The key function of the cyclone here, apart from separating the particulate, is to accelerate the flow towards the fabric filters, which are located in the central part where the vortex finder is usually located.
The basic principles of filtration can be traced back to those that regulate the general motion of fluids in porous media.
A porous medium is characterized by a partitioning of the total volume into solid matrix and pore space, with the latter being filled by the fluid.
The basic feature of this medium is porosity. The bulk porosity Π of a material is defined as the ratio of void volume V_v to body volume V_0:

$$\Pi = V_v/V_0 \quad (4).$$

Since the remaining portion V_s of the total volume of the material is in the form of a solid matrix, then:

$$1 - \Pi = V_s/V_0 \qquad (5).$$

Permeability (or gas permeability) is the property that gives a measure of the gas flow through a porous medium exposed to a pressure difference. The superficial velocity V of the fluid flow depends on permeability and pressure gradient in accordance with a Darcy's law.
At laminar flows, the inertia term in the Darcy's equation may be neglected and the equation takes the form that is widely used in the theory of filtration:

$$\frac{dp}{dx} = \frac{\mu}{K} \cdot v \qquad (6)$$

where $K = 1/\alpha$ is the Darcy's permeability coefficient in [m^2] and α is the permeability [1/ m^2].
The inertia term is instead needed in presence of turbulent flows: in this scenario, the equation becomes:

$$\frac{dp}{dx} = \frac{\mu}{K} \cdot v + \rho \cdot \frac{K_{loss}}{2} \cdot v^2 \qquad (7)$$

where $\frac{K_{loss}}{2} = 0{,}043(1-\alpha)^{-2{,}13}$ [ANSYS FLUENT 18 – Theory Guide].
The difference between Equation 6 and 7 is clarified in Figure 5.

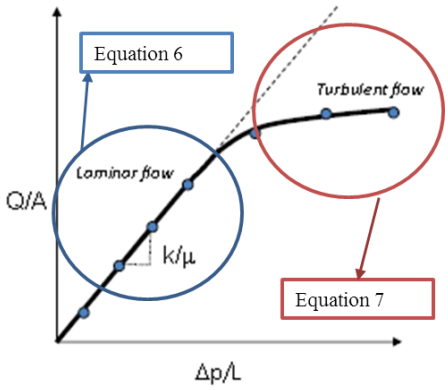

Figure 5: Difference between the Darcy's equations.

3. COMPUTATIONAL FLUID DYNAMICS MODEL

3.1. Geometry

The computational geometry reproduced the sizes of the bag filter in the pilot plant, with the details of the filter hoses positions (Figure 6).

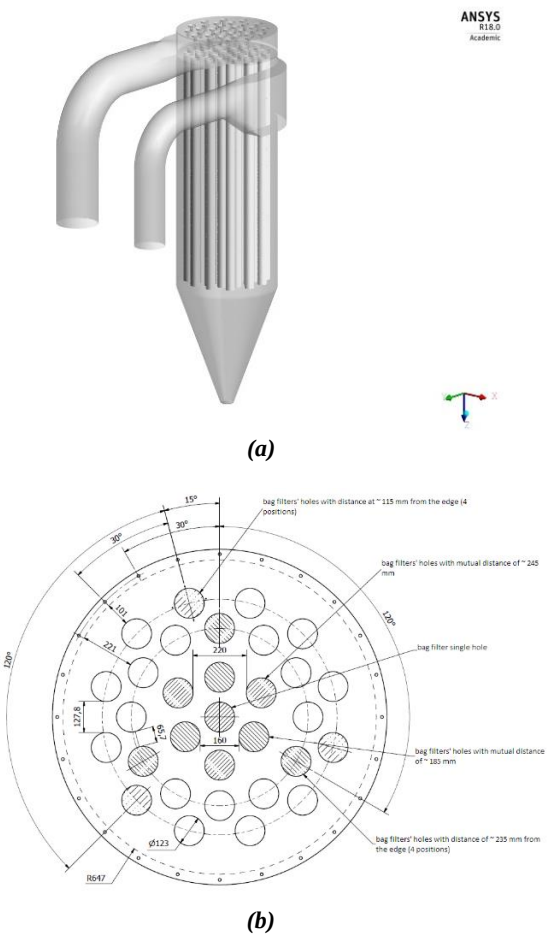

Figure 6: Computational domain (a) and bag filters positions (b).

To obtain a fully developed flow, both the inlet and the outlet ducts were lengthened with the aim to avoid as much as possible the undeveloped flow disturbance. The dimension are shown in Table 4.

Cyclone total height	5308 mm
Cyclone diameter	1300 mm
Cyclone conical height	1550 mm
Cyclone conical min. diameter	168 mm
Bag filters height	3000 mm
Bag filters diameter	123 mm
Fabric filter hoses	31

Table 4: Domain sizes.

3.2. Volume discretization techniques

The domain was discretized with Ansys MESHING, based on the Finite Volume Method.
To be specific, a fine mesh was chosen in correspondence to the fabric filters to capture the velocities that cross the small gaps in-between them successfully.
Table 5 shows the mesh specifications and Figure 7 sketches the mesh structure.

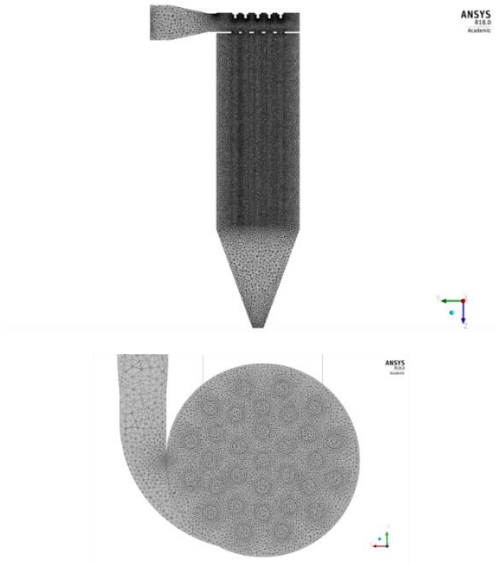

Figure 7: Computational domain.

Element Type	Tetrahedrons
Num. Elements	21499727
Num. Nodes	3673564
Max. Size	0.06 m
Curvature	10°
Edge Sizing	0.01 m
Growth Rate	1.1

Table 5: Mesh specifications.

3.3. Solver settings

Four simulations were carried out in Ansys FLUENT 17.0 in a steady-state condition, at the following inlet velocities: 15 m/s, 19 m/s, 22.5 m/s and 25 m/s. The atmospheric pressure was set at the outlet.

3.3.1. Turbulence model k-ε

To represent the fluid motion inside the filter accurately, the Realizable k – ε turbulence model was chosen.

The k – ε model is one of the most common turbulence models, although it just does not perform well in cases of large adverse pressure gradients. It is a two-equation model, which means it includes two extra transport equations to represent the turbulent properties of the flow. This allows a model to account for history effects like convection and diffusion of turbulent energy.

The first transport variable *k* is the turbulent kinetic energy. The second transport variable *ε* is the turbulent dissipation. The latter determines the scale of the turbulence, whereas the former, k, determines the energy in the turbulence.

As said before, the k – ε model it is useful for free-shear layer flows with relatively small pressure gradients.

For the Realizable k – ε, the model transport equations are:

$$\underbrace{\rho U_i \frac{\partial k}{\partial x_i}}_{\text{Convection}} = \underbrace{\mu_t S^2}_{\text{Generation}} + \underbrace{\frac{\partial}{\partial x_i}\left(\alpha_k \mu_{\text{eff}} \frac{\partial k}{\partial x_i}\right)}_{\text{Diffusion}} - \underbrace{\rho\varepsilon}_{\text{Dissipation}} \tag{8}$$

for the kinetic energy and

$$\underbrace{\rho U_i \frac{\partial \varepsilon}{\partial x_i}}_{\text{Convection}} = \underbrace{C_{1\varepsilon}\left(\frac{\varepsilon}{k}\right)\mu_t S^2}_{\text{Generation}} + \underbrace{\frac{\partial}{\partial x_i}\left(\alpha_\varepsilon \mu_{\text{eff}} \frac{\partial \varepsilon}{\partial x_i}\right)}_{\text{Diffusion}} - \underbrace{C_{2\varepsilon}\rho\left(\frac{\varepsilon^2}{k}\right)}_{\text{Destruction}} - \underbrace{\underline{R}}_{\substack{\text{Additional term}\\ \text{related to mean strain}\\ \text{\& turbulence quantities}}} \tag{9}$$

for the dissipation rate. Both equations are written for steady, incompressible flow without body forces [ANSYS FLUENT 18 – Theory Guide].

3.3.2. Fabric filter characterization

For what concerns the representation of the filter, the porous jump option was activated in Ansys FLUENT using the parameters in Table 6.

Permeability	$6.72 \cdot 10^{-11}$ m^2
Thickness	0.0014 m
Pressure coefficient	0

Table 6: Porous jump parameters.

These values were calculated from the air permeability curve provided by the filter manufacturer (Figure 8), evaluating:

$$\frac{1}{\alpha} = \frac{\Delta p}{w\, \mu_{air}\, s} \tag{10}$$

where w is the flow rate in [l/(dm²min)], Δp is the pressure drop introduced by the filter, μ_{air} is the air viscosity and s is the thickness of the filter surface.

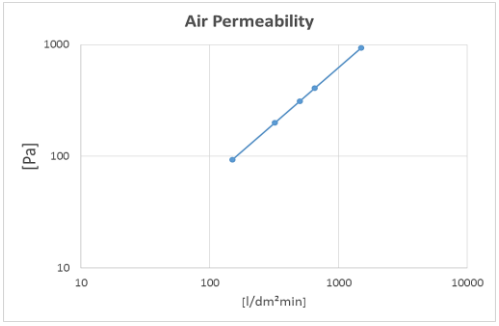

Figure 8: Air permeability curve.

Porous jump conditions are used to model a thin membrane that has a known velocity (pressure-drop) characteristics. It is essentially a 1D software simplification of the porous media model available for cell zones. Examples of uses for the porous jump condition include modeling pressure drops through screens and filters. This simpler model should be used whenever possible because it is more robust, yields better convergence and shortens the computational time.

The thin porous medium (porous jump) has a finite thickness over which the pressure change is defined as a combination of Darcy's law and an additional inertial loss term:

$$\Delta p = -\left(\frac{\mu}{\alpha} v + C_2 \frac{1}{2} \rho v^2\right) \Delta m \qquad (11)$$

where μ is the laminar fluid viscosity [Pa·s], α is the permeability [m^2], C_2 is the inertial pressure-jump coefficient [1/m], ρ is the fluid density [kg/m^3], v is the velocity normal to the porous face [m/s] and Δm is the thickness of the medium [m] [ANSYS FLUENT 18 – Theory Guide].

4. RESULTS AND MODEL VALIDATION

The simulations were performed at 15 m/s, 19 m/s, 22.5 m/s and 25 m/s. The results showed a correct representation of the behavior of the bag filter, as it can be seen by observing the velocity contours in Figure 9.

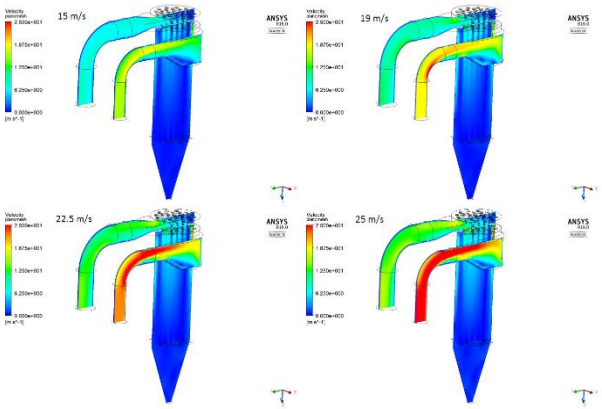

Figure 9: Inlet sensors positions.

Afterwards, the results were compared with the experimental data.
In particular, the comparison focused on inlet and bottom velocities together with the pressure drop.

4.1. Filter inlet velocities

The cyclone inlet velocities were evaluated at the four yellow points in Figure 2, whose detailed positions are shown in Figure 10.

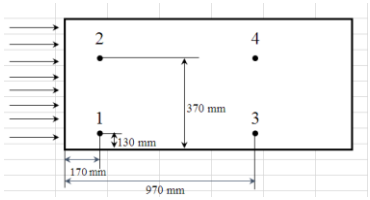

Figure 10: Inlet sensors positions.

The four positions have been chosen to capture the entire fluid flow accurately. The hot-wire anemometer was positioned at different distances from the external volute wall (Figure 11), 5 cm, 15 cm and 29 cm, and for each distance the maximum and the minimum velocity value was measured (Figure 11).

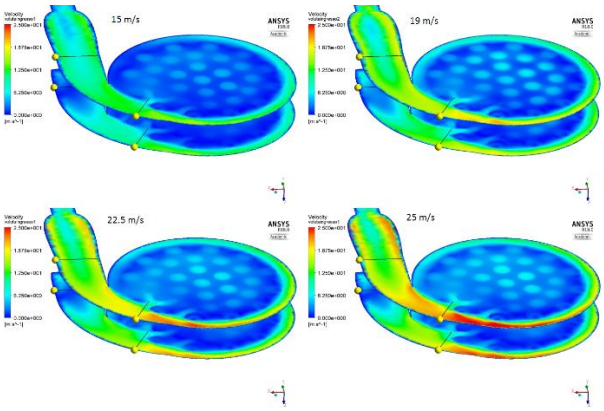

Figure 11: Inlet velocity magnitude contours and the collection points.

Table 7 lists the results obtained for each point at different depth. For the sake of brevity, only the values related to 15 m/s e 22.5 m/s are displayed.

	15 m/s							
	point 1		point 2		point 3		point 4	
	x [cm]	v [m/s]	x [cm]	v [m/s]	x [cm]	v [m/s]	x [cm]	v [m/s]
min	5	2.00	5	9.00	5	10.00	5	11.50
max		4.00		11.00		12.00		13.50
min	15	0.10	15	6.00	15	7.00	15	9.50
max		2.00		10.00		9.00		11.50
min	29	2.50	29	3.00	29	4.00	29	1.50
max		3.50		4.00		6.00		3.00
	22,5 m/s							
	point 1		point 2		point 3		point 4	
	x [cm]	v [m/s]	x [cm]	v [m/s]	x [cm]	v [m/s]	x [cm]	v [m/s]
min	5	3.00	5	15.00	5	15.00	5	17.50
max		5.50		17.00		18.00		20.00
min	15	0.01	15	10.00	15	10.00	15	14.00
max		2.00		12.00		14.00		17.00
min	29	4.00	29	4.00	29	5.00	29	4.50
max		6.00		5.50		8.00		7.00

Table 7: Cyclone inlet velocities at different inlet velocity.

The collected values showed a good correspondence with those returned from the simulations. The curves in Figure 12 and 13 are included, in fact, between the maximum and the minimum experimental value.

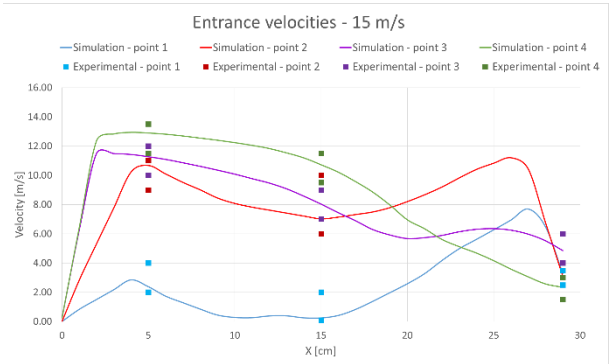

Figure 12: Volute velocities at 15 m/s. Comparison between experimental and simulations data.

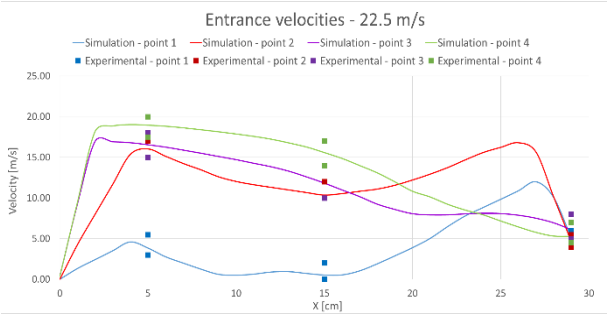

Figure 12: Volute velocities at 22.5 m/s. Comparison between experimental and simulations data.

Again, only the values at 15 m/s and 22.5 m/s are shown for simplicity purpose.
As a result, the inlet distribution of velocity was successfully validated.

4.2. Bottom velocities

The next stage was the collection of the velocity data in the conical part of the filter, i.e. its bottom, in this case as well, these data were gained using the hot-wire anemometer at the point highlighted in Figure 14, which also shows the vertical velocity vectors.

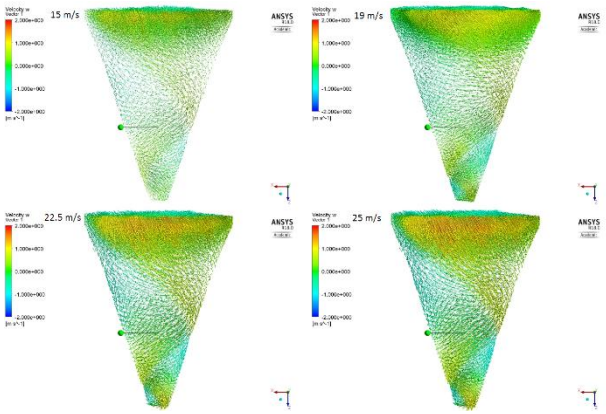

Figure 14: Bottom velocity vectors with the collection point.

Once again, the maximum and minimum velocity values were collected at different distances from the external wall and at each inlet velocity (Table 8).

Bottom velocities [m/s]				
		10 cm	20 cm	30 cm
15 m/s	min	0.01	0.01	0.01
	max	0.08	0.1	0.06
22.5 m/s	min	0.1	0.01	0.07
	max	0.25	0.1	0.2

Table 8: Cyclone bottom velocities at different inlet velocity.

Figure 15 illustrates the comparison between the experimental and the simulations values. It is clear that the maximum and minimum values include the curves extracted from the simulations, thus validating the model with respect to the bottom velocities.

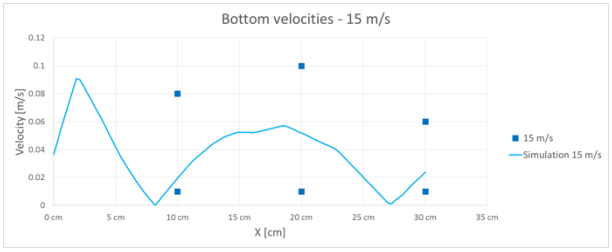

(a)

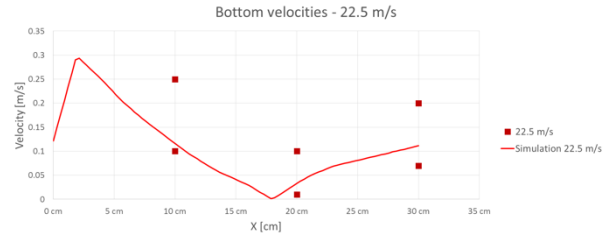

(b)

Figure 15: Bottom velocities comparison at (a) 15 m/s and (b) 22.5 m/s.

4.3. Pressure drop

The evaluation of the pressure drop was made thanks to the differential pressure sensor by measuring the inlet and the outlet pressure of the bag filter and then calculating the pressure drop as the difference between the previous two.
Table 9 illustrates the experimental pressure drops coupled with the velocities detected at the inlet duct with the Pitot tube sensor. In the same table, the computational results are collected to make the comparison easier.

Collected data		Simulated data	
Pitot velocity [m/s]	Δp [Pa]	Velocity [m/s]	Δp [Pa]
15.4	208	15	175
18.8	297	19	256
22.1	416	22.5	340
24.6	426	25	405

Table 9: Pressure drop values.

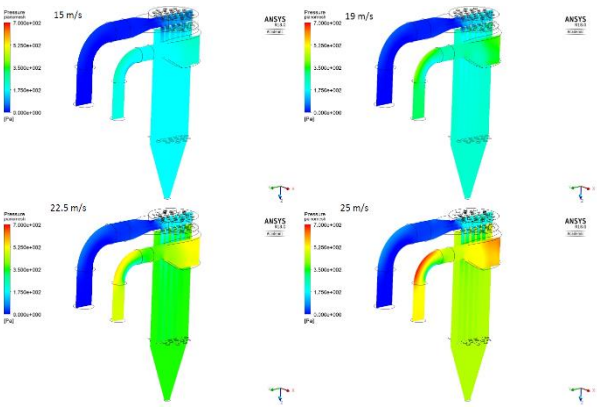

(a)

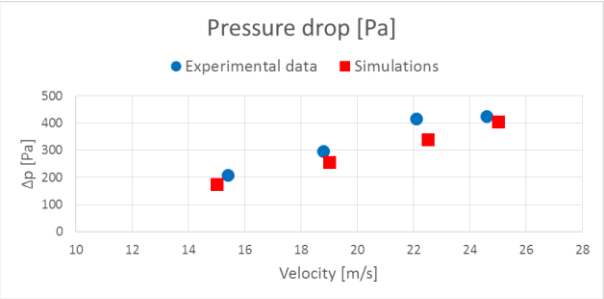

(b)

Figure 16: Pressure drop values (a) contours and (b) comparison.

As the chart in Figure 16 (b) shows, the pair of values from the sensors are very close to those from the simulations. This confirms that the one presented is a robust model for predicting the bag filter operating conditions, thus validating it once again.

5. CONCLUSIONS

The objective of this work was to study the behavior of a combined air filtration system consisting in a cyclone separator and a bag filter with 31 hoses.

The performance of such system was analyzed at different operating conditions with the purpose to obtain a predictive model for industrial design.

This was possible due to computational fluid dynamics simulations, which were validated with a dedicated experimental campaign on a pilot plant.

The first step of the study focused on the sensor placement, for the velocity and pressure data acquisition. The housings were created for the sensors probes along the filter as well as at the inlet and outlet ducts (Figure 2).

A hot-wire anemometer and a Pitot tube flow meter were used to measure the velocity data, while the pressure drop was collected using a differential pressure sensor.

To check the good response of the pilot plant, the airflow rates were acquired experimentally and compared with the ones from the fan operating curve at different inverter frequencies.

After the data acquisition, the 3D model of the bag filter was implemented. The model discretization inside Ansys MESHING considered the small gaps between the filter hoses, thus a fine mesh was created to capture the velocity field in those zones correctly.

Next, CFD simulations were carried out in a steady state, at the following inlet velocities: 15 m/s, 19 m/s, 22.5 m/s and 25 m/s.

The model validation was performed by comparing the simulations results with the data collected by the sensors, considering both the velocities (at the inlet and at the bottom) and the pressure drop inside the filter.

For the volute and the bottom velocities, a maximum and a minimum value was measured with a hot-wire anemometer. Thereafter, it was checked if the velocity curves from the simulation were included between the two experimental values.

The results of this comparison were satisfying, therefore the model could be validated from the velocity field point of view.

Regarding the pressure drop, a differential pressure sensor gauged the experimental data, in correspondence to the inlet velocities, collected with a Pitot tube. These pair of values were confronted with the ones from the simulations.

This comparison showed a good response of the computational model too, confirming its validation.

Finally, the project goal was achieved successfully and a predictive fluid dynamic model for the design of the filtration pilot plant was obtained.

Further developments will involve the analysis of the piping from the fluid dynamics point of view (velocities and pressure drop) and the model scale-up for the operating conditions simulation of the industrial plant.

REFERENCES

Alexander, R. M. C. K., (1949). Fundamentals of Cyclone Design and Operation. Australian Institute of Minerals and Metallurgy, 152; 203 – 28.

ANSYS FLUENT 18 – Theory Guide.

ANSYS FLUENT 18 – User Guide.

Billings, C. E., Wilder, J., (1970). Handbook of Fabric Filters Technology – Volume 1. GCA Corporation, Bedford, Massachusetts.

Chen, J., Shi, M. (2007). A Universal Model to Calculate Cyclone Pressure Drop. Powder Technology, 171, 184 – 191.

Cortés, C., Gil, A., (2007). Modeling the Gas and Particle Flow inside Cyclone Separators. Progress in Energy and Combustion Science, 33, 409 – 452.

De Brito Dias, D., Mori, M., Martignoni, W. P., (1997). Study of Different Approaches for Modeling Cyclones Using CFD. University of Campinas, Campinas, SP, Brazil.

Endress – Hauser Deltabar S PMD75 Manual.

Hanakalic, K., (2004). Closure Models for Incompressible Turbulent Flows. Introduction to Turbulence Modeling. Von Karman Institute for Fluid Dynamics, 1 – 75.

KIMO DEBIMO 400 Air Flow Measuring Blades Manual.

Le Goff, P., Leclerc, D. M., Herzig, J. P., (1969). Flow Suspensions through Porous Media. Industrial and Engineering Chemistry.

Lo, L. M., Chen, D. R., Pui, D. Y. H., (2009). Experimental Study of Pleated Fabric Cartidges in a Pulse – Jet Cleaned Dust Collector. Powder Technology, 197, 141 – 149.

Mehta, N. C., Smith, J. M., Comings, E. W., (1956). Pressure Drop in Air – Solid Flow Systems. Fluid Mechanics in Chemical Engineering.

Meier, H. F., Mori, M., (1998). Gas – Solid Flow in Cyclones: the Eulerian – Eulerian Approach. European Symposium on Computer Aided Process Engineering.

Patankar, N. A., Joseph, D. D. Modeling and Numerical Simulation of Particulate Flows by the Eulerian – Lagrangian Approach. Department of Aerospace Engineering and Mechanics, Northwestern University, Evanston.

Sommerfeld, F., (2000). Theoretical and Experimental Modelling of Particulate Flows. Von Karman Institute for Fluid Dynamics.

Stendal, E. A. R. (2013). Multiphase Flows in Cyclone Separators. Department of Chemical Engineering, Gothenburg, Sweden.

Sutherland, K., (2008). Filters and Filtration Handbook – 5th Edition. Elsevier Science.

Ter Linden, A. J., (1949). Investigation into Cyclone Dust Collectors. Institute of Mechanical Engineering, 160; 233 – 51.

VelociCalc Air Velocity Meter 9565 Series.

Yoa, S. J., Cho, Y. S., Choi, Y. S., Baek, J. H., (2001). Characteristics of Electrostatic Cyclone/Bag Filter with Inlet Types (Lab and Pilot Scale). Korean Journal of Chemical Engineering, 18, 539 – 546.

AUTHORS BIOGRAPHY

Federico SOLARI is a PhD in Industrial Engineering at the University of Parma, from where he got a Master Degree in Food Industry Mechanical Engineering, discussing a thesis related to the design of a plant for the volatile compounds extraction. He achieved his PhD with a thesis entitled “Advanced approach to the design of industrial plants by means of computational fluid dynamics”. He attended several conferences related to food process, modelling and simulation. He published several papers on the same topics on international journal and conferences.

Giorgia TAGLIAVINI is a Research Assistant at the Department of Industrial Engineering at the University of Parma, where she graduated in Mechanical Engineering in March 2015. Her research activities focus mainly on CFD simulation of multiphase flows and non-Newtonian fluids, data analysis and modeling of Fluid Mechanics and Industrial Engineering processes.

Roberto MONTANARI is Full professor of Mechanical Plants at the University of Parma. He graduated (with distinction) in 1999 in Mechanical Engineering at the University of Parma. His research activities mainly concern equipment maintenance, power plants, food plants, logistics, supply chain management, supply chain modelling and simulation, inventory management. He has published his research in approx. 70 papers, which appear in qualified international journals and conferences. He acts, as a referee, for several scientific journals, is editorial board member of two international scientific journals and editor of a scientific journal.

Eleonora BOTTANI is Associate professor in Mechanical Industrial Plants at the Department of Engineering and Architecture of the University of Parma. She graduated (with distinction) in Industrial Engineering and Management in 2002, and got her Ph.D. in Industrial Engineering in 2006, both at the University of Parma. Her research activities concern logistics and supply chain management issues. She is author (or co-author) of more than 130 scientific papers, referee for more than 60 international journals, editorial board member of five scientific journals, Associate Editor for one of those journals, and editor-in-chief of a scientific journal.

Nicola MALAGOLI is a Research Assistant at the Department of Industrial Engineering at the University of Parma. He has a Master Degree in Food Industry Mechanical Engineering in October 2016. His research activities focus mainly on data analysis and food industry plants design.

Mattia ARMENZONI is a Research Assistant in Industrial Engineering at the University of Parma. He got a master degree in Food Industry Mechanical Engineering, discussing a thesis titled: "Advanced design of a static dryer for pasta with simulation tools". He attended several international conferences and published several papers related to food industry, modelling and simulation.